Optical and transport properties and the structural identification of $IrTe_2$

Kyoo Kim,[1,2,*] Sooran Kim,[1] and B. I. Min[1,†]

[1]*Department of Physics, Pohang University of Science and Technology, Pohang 790-784, Korea*

[2]*c_CCMR, Pohang University of Science and Technology, Pohang 790-784, Korea*

(Received 11 August 2014; revised manuscript received 21 October 2014; published 19 November 2014)

$IrTe_2$ exhibits a structural phase transition at $T_s \sim 280$ K. Utilizing the density functional theory, we have simulated optical spectra above and below T_s. Simulated optical absorption spectra for a specific (5X) structure show great agreement with experimental data below T_s, which provides the structural identification of $IrTe_2$ at low temperature. Comparison between experimental and calculated optical spectra also indicates that the Ir-Ir dimer formation governs the optical transition over the wide energy window of the low frequency part. The analysis of Fermi surfaces and band dispersions supports the effects of dimerization on the optical spectra at the low frequency region. The conductivity calculation based on the Boltzmann transport theory within the constant relaxation time approximation reveals that the dimensional reduction as well as the change of conducting plane takes place during the structural transition of $IrTe_2$.

DOI: 10.1103/PhysRevB.90.195136 PACS number(s): 71.30.+h, 71.45.Lr, 72.15.Eb, 78.20.−e

I. INTRODUCTION

Transition-metal dichalcogenide (TMDC) systems have varieties of interesting properties, such as superconductivity, thermoelectricity, ferroelectrics, charge density wave (CDW), and/or an interplay among them [1–5]. Such an interplay leads to a phenomenon called the quantum criticality, in which the ground state of the system can be easily tuned with external parameters such as doping, magnetic field, and pressure. Moreover, the structures of most TMDC systems possess layers, which are weakly connected by the van der Waals interaction. Therefore they can be easily made into single layers called skinny, or one can intercalate atoms inside the layers. Due to the unique layered structure, TMDC has a great possibility in the field of industrial applications. After the recent discovery of superconductivity in doped $IrTe_2$, which is a TMDC of CdI_2, by Yang *et al.* [6], there have been lots of efforts to understand the mechanism of the structural transition in $IrTe_2$ and its complicated phases. $IrTe_2$ exhibits the rich phase diagram with doping and temperature (T). Undoped $IrTe_2$ has an abrupt first order structural transition near $T_s \sim 280$ K to a $q_{1/5} = (1/5,0,1/5)$ modulated structure (5X) [6]. As with Pt or Pd doping, T_s is reduced, and with further doping, the structural transition disappears and the superconducting phase emerges near the quantum critical point [6]. The interplay between the structural transition and the superconductivity draws lots of attention to pursue new phases of matter. Therefore the structural information on the undoped $IrTe_2$ and the understanding of the mechanism of structural transition is prerequisite to investigate its exotic phenomena.

A number of scenarios have been proposed for the structural transition, such as charge/orbital density wave,[6] orbital-induced Peierls instability [7,8], crystal-field effect of Te p orbital [9–11], anionic depolymerization transition [12], and so on. But the origin of structural transition in $IrTe_2$ is still under debate.

Optical measurements on $IrTe_2$ were performed by Fang *et al.* [9]. Their T-dependent optical spectra indicated the heavy reconstruction of band structure upon cooling. But they argued that they did not find any signature of the CDW state proposed by Yang *et al.* [6]. They adopted the density functional theory (DFT) to analyze their experiment and claimed that Ir 5d t_{2g} orbitals are fully occupied both above and below T_s and so do not participate in the structural transition. Hence they concluded that Te p orbitals are responsible for the structural transition. However, their analysis was based on the monoclinic structure reported by Matsumoto *et al.* [13], which did not count $q_{1/5} = (1/5,0,1/5)$ modulation (5X) of $IrTe_2$ at low T [6].

Recently, Pascut *et al.* [14] refined the modulated structure as a triclinic one by using x-ray diffraction. With the help of DFT/DMFT calculations, they argued that the dimer formation of Ir is the main mechanism of the structural transition in $IrTe_2$. Ir3 atoms, which form dimers, have more hole carriers, and there is indeed experimental evidence of the Ir charge order/disproportionation [7,12,15,16]. The structural information by Pascut *et al.* seems to be consistent with experiments, such as extended x-ray absorption fine structure (EXAFS) [17], angle resolved photoemission spectroscopy (ARPES) [18], quantum oscillation [19]. Joseph *et al.* [17], from EXAFS measurement, found the order-disorder like Ir-Ir dimer formation. Kim *et al.* [18] found the great agreement between ARPES and DFT bands calculated for a triclinic structure of $IrTe_2$, and found that the Ir dimer formation contributes to the strong reconstruction of band structures near the Fermi level (E_F). Eom *et al.* [19] found a good agreement between the experimental and theoretical Fermi surface topology, from the quantum oscillation experiment.

Nevertheless, the low T structure of $IrTe_2$ has not been fully settled yet. According to a very recent report by Li *et al.* [20], the low T structure of IrTe2 was identified to have $C2/m$ type symmetry, which is quite similar to the one suggested by Matsumoto *et al.* [13]. Therefore, experimental and theoretical confirmations of the low T structure of $IrTe_2$ are urgently demanded for further study of $IrTe_2$. The DFT-based simulation of optical spectra for a low T structure with $q_{1/5}$ modulation has not been available yet. Therefore, in this paper,

*kyoo@postech.ac.kr
†bimin@postech.ac.kr

using the structural data refined by Pascut *et al.* [14], we have simulated and analyzed optical spectra of $IrTe_2$ both above and below T_s. We have obtained the consistent results between the calculation and the experiment for a structure having Ir-Ir dimer formation. We have also calculated the electrical conductivity of $IrTe_2$ below T_s, which shows the good agreement with experiment.

II. COMPUTATIONAL DETAILS

We have used the full-potential linearized augmented plane wave band method with local orbitals, implemented in the WIEN2K [21]. For the exchange-correlation potential, the PBE has been used. To take into account the relativistic effects of Ir and Te, the spin-orbit interaction is included in a second variational manner with a large enough energy window up to 5 Ry. We have simulated optical spectra using the optic package within WIEN2K [22], for the high T hexagonal structure (HEX), hypothetical low T monoclinic structure used by Fang *et al.* (hMONO) [9,13], and low T modulated structure refined by Pascut *et al.* (5X) [14], as shown in Fig. 1. We provide a side view of 5X structure in Fig. 1(d), to show the dimer ordering of 5X structure explicitly. Note that the hMONO structure is similar to HEX, but the hexagonal c axis is inclined to the hexagonal a direction, and the lattice is compressed along the a direction, and so shortened bonds are formed along the a direction uniformly [9]. The calculations for the electrical conductivity were carried out with the Boltzmann transport method implemented in BoltzTraP [23].

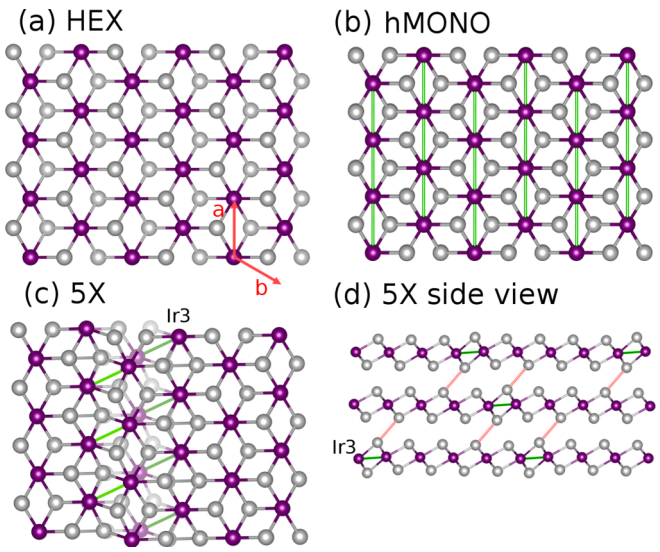

FIG. 1. (Color online) Crystal structures of $IrTe_2$ [(a)–(c): top views, (d): side view]. Violet (gray) sphere represents Ir (Te) atom. (a) High T hexagonal structure (HEX). Hexagonal unit cell vectors a and b are depicted with red arrows. (b) Hypothetical low T monoclinic structure (hMONO) employed by Fang *et al.* (Ref. [9]) which corresponds to averaged structure with uniform shortened Ir bonds along the a direction. (c) Low T $q_{1/5} = (1/5, 0, 1/5)$ modulated structure (5X). (d) Side view of the 5X structure. The 5X structure has Ir-Ir dimers together with Te-Te short bonds. Rods with green (red) color indicate Ir-Ir (Te-Te) shortened bonds. The iridium atoms forming dimers are denoted as Ir3, following Pascut *et al.*'s convention (Ref. [14]).

III. RESULTS AND DISCUSSIONS

1. Optical Spectra

Figure 2(a) presents the simulated reflectivities as a function of frequency for HEX, hMONO, and 5X structures, and Fig. 2(c) presents the experimentally observed reflectivities at $T = 200$ and 300 K. The experimental reflectivity at $T = 300$ K shows a reflectivity edge at $\omega \simeq 0.5$ eV and a shallow dip near $\omega = 1.5$–2.0 eV, which are characteristic features of a good metallic system [24]. On the other hand, there is a sudden drop of reflectivity for $T = 200$ K data, which indicates the decrease of metallic character at low T. It happens because of the partial gap opening through the formation of dimer ordering. Figure 2(a) and 2(c) manifest that the simulated data with HEX (5X) structure capture the characteristics of high (low) T experimental data quite well. On the contrary, the hMONO structure cannot capture the reduction of reflectivity at low T. Since the hMONO structure corresponds to a kind of averaged structure of 5X without dimer ordering, we can deduce that Ir dimer formation is responsible for the low frequency behavior of reflectivity.

In Figs. 2(b) and 2(d) are presented the calculated and experimental data for the real part of optical conductivity σ_1, which corresponds to the absorption spectrum. Reduction of the Drude weight and increase of the high frequency shoulder near 2.0 eV are observed experimentally upon cooling. Here again, excellent agreement is obtained at low T with 5X structure. As reported by Kim *et al.* [18], the disappearance of one lobe of the Fermi surfaces reduces the DOS near E_F, resulting in the reduction of the Drude peak. The good agreement between experimental and DFT-calculated optical spectra reveals that the low T structure of $IrTe_2$ can be identified with the 5X structure refined by Pascut *et al.* [14]. Therefore the dimer formation of Ir is responsible for the band structure reconstruction over a wide energy window around E_F, and so the optical transition in the low frequency part.

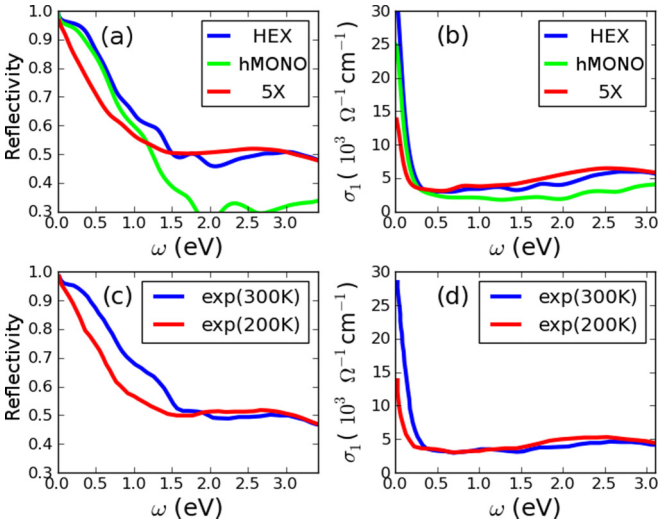

FIG. 2. (Color online) Theoretical reflectivity (a) and absorption spectra (σ_1) (b) for HEX (blue), hMONO (green), and 5X (red) structures. Experimental reflectivity (c) and absorption spectra (d) measured at $T = 300$ K (blue) and $T = 200$ K (red) [9].

TABLE I. The RMS values for the plasma frequencies for HEX, hMONO, and 5X structures of $IrTe_2$, which are compared with experimental ones. [9] Note that the plasma frequency changes depending on the direction of incident light.

Plasma frequency	$\omega_P^{RMS/EXP}$ [eV]
HEX	4.518
hMONO	4.108
5X	3.065
EXP($T = 300$ K)	4.841
EXP($T = 250$ K)	3.624

In Table I, calculated and observed plasma frequencies are provided. It is hard to compare calculated and observed plasma frequencies directly because the orientation of incident light is not specified in the literature [9]. For HEX, the in-plane component of plasma frequency would be important. But it is hard to get ω_P for a specific direction, especially for 5X, for which the crystal axes are tilted against the HEX axes. Thus we considered the root mean square (RMS) values of directional plasma frequencies for comparison with experimental results. It shows that, for hMONO, the reduction of plasma frequency is about 9% with respect to that of HEX, while for 5X it is 32%. Experimentally, it is 25%. Therefore, the plasma frequency reduction in $IrTe_2$ upon cooling is properly described by the structural transition from HEX to 5X too.

As mentioned earlier, Fang *et al.* [9] claimed that the Te p orbitals play a dominant role in the structural deformation, based on the wrong structure that does not contain the periodic lattice modulation. So they considered only the uniform suppression of lattice constant along the a axis, but did not account for the charge ordering of Ir ions with the period of $q_{1/5} = (1/5,0,1/5)$. Since the dimer formation in 5X is closely related to the charge ordering of Ir [14,18], the great agreement of experimental and simulated results of optical spectra for 5X structure indicates that the noticeable T-dependent change of the optical spectra comes from the band reconstruction via the Ir dimer formation. In fact, the Ir3-Ir3 dimer ordering is thought to be formed via a molecular orbital version of the Jahn-Teller distortion in the Ir3-Ir3 stripe generated by $q_{1/5}$ periodic modulation [18].

2. *Band dispersions and Fermi surfaces*

The change in the optical spectra can be understood with the help of band dispersions and Fermi surfaces (FSs) obtained with DFT calculation. To investigate the change of FSs during the structural transition, we have constructed a five times large supercell of HEX unit cell (HEX5 hereafter), which has the same symmetry as 5X unit cell.

The optical spectra in the low frequency part can be well described by the band dispersions in Figs. 3(a) and 3(b). For 5X structure, there are newly-appeared flat bands near 0.75 and −0.25 eV which give optical transitions in the frequency scale of ∼1 eV. This observation is consistent with reflectivity and absorption data in Fig. 2. Note that the newly-appeared bands mostly come from dimerized Ir orbitals.

In Fig. 3(d), FSs of HEX5 and 5X are shown together. By taking HEX5 as a unit cell instead of HEX, bands are folded

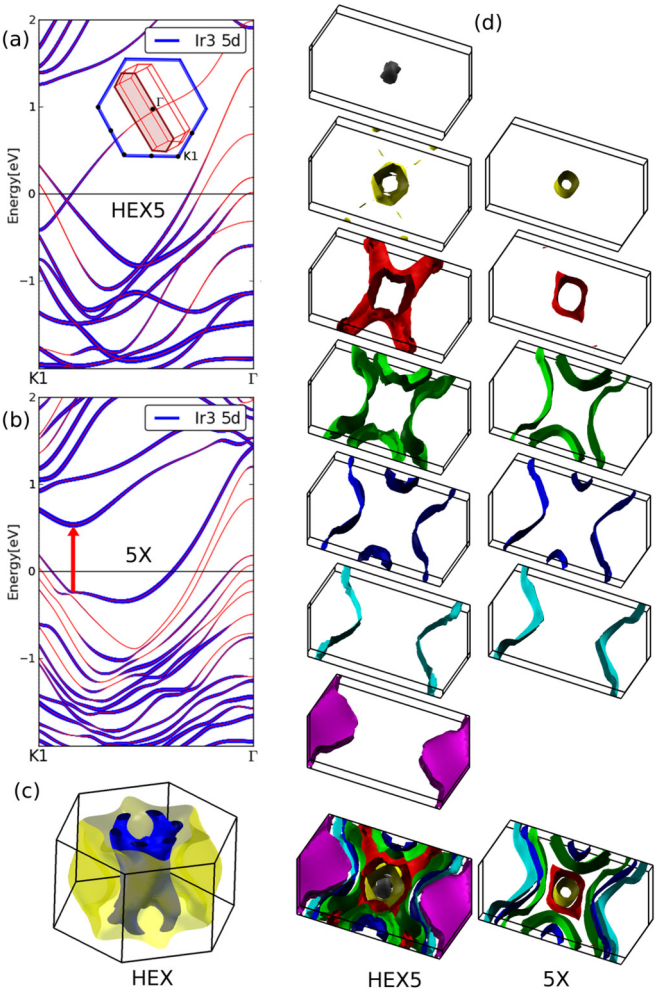

FIG. 3. (Color online) (a) band dispersion of high T phase of HEX $IrTe_2$, which are folded into the BZ of 5 times larger hexagonal supercell (HEX5). (b) band dispersion of low T phase of 5X. For the band dispersion, Ir3 $5d$ orbital projection is shown together. Red arrow for 5X indicates the dominant optical interband transition (about 0.8 eV). The inset in (a) shows the smaller BZ of HEX5 (and 5X) inside the larger BZ of HEX. (c) Fermi surfaces (FSs) of high T phase of HEX $IrTe_2$ without considering the band folding. (d) Band decomposed FSs of HEX5 and 5X structures. FSs in the same row correspond to those with the same band indices. Last rows of each column are total FSs. Note that the first and seventh rows of 5X FSs are missing.

into a smaller Brillouin zone (BZ) of HEX5, resulting in the complicated FSs, as shown in Fig. 3(d). We have used the same colors for the FSs with the same band indices for HEX5 and 5X. Note that there are two FSs (inner/outer FSs) for the HEX BZ, and the outer FS has three lobes, as shown in Fig. 3(c). When folded, those two FSs produce rather complicated FSs for the HEX5 BZ. In Fig. 3(d), one can easily identify X-shaped FSs (green, blue, cyan) in both HEX5 and 5X. They and the violet FS arise from the folded lobes of outer FS of the HEX BZ [yellow FS in 3(c)]. There are also small tube-shaped FSs around Γ (gray, yellow, red), which arise from the inner FS of the HEX BZ [blue FS in Fig. 3(c)]. Under the structural transition to 5X, there are mainly two changes. The first one is

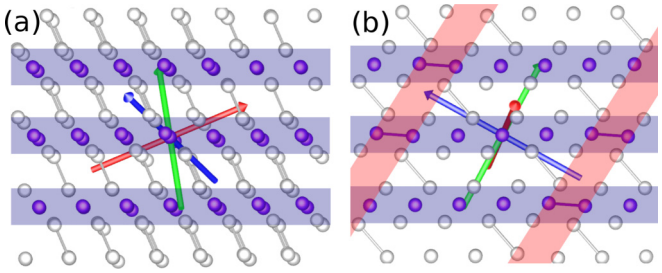

FIG. 4. (Color online) Principal axes for the conductivity tensor σ. Green, red, and blue arrows indicate three principal axes of the 5X structure. (a) and (b) are the directional views, which show red and blue arrows more clearly. Violet (white) sphere represents Ir (Te) atom, and rods that connect atoms represent shortest bonds. Gray shaded regions denote $IrTe_2$ layers, while red shaded regions denote layers with Ir3-Ir3 dimer ordering. The conductivity ratio among principal values along the green, red, and blue arrows is obtained to be 1.99: 3.86: 0.57. Note that the blue arrow that is almost perpendicular to red shaded layers corresponds to the principal axis having the smallest conductivity.

the disappearance of gray and violet FSs (the first and seventh rows of HEX5 data). The second one is the large deformation of tube shaped FSs (red). Noteworthy is that X-shaped FSs do not change much, while the violet FS disappears, which means that only one lobe (violet FS) out of the outer three FSs disappears. The disappearance of violet FS is mainly responsible for the reduction of DOS at E_F: It reduces about 1/3 of DOS at E_F.

3. *Electrical conductivity*

We expect that there will also be a large change in the electrical conductivity in $IrTe_2$ during the structural transition due to substantial band reconstruction near E_F. Directional gap opening indicates that there might be a change of conducting plane, as suggested by Toriyama *et al.* [25]. Using BoltzTraP, we have calculated conductivity of $IrTe_2$, below and above T_s [23]. For HEX structure, the ratio of principal values of conductivity tensor is about 4.98 : 4.32 : 2.53, which reflects nearly three-dimensional (3D) character at high T phase of $IrTe_2$. For 5X structure, the conductivity tensor has a large portion of the off-diagonal terms in the basis unit cell vector. Therefore we diagonalized the conductivity tensor to obtain principal axes. Principal axes for 5X structure is shown in Fig. 4 as green, red, and blue arrows. The ratio of principal values of conductivity tensor is about 1.99 : 3.86 : 0.57 (green : red : blue). The ratio of the largest principal values of conductivity between HEX and 5X structure is about 5:4.

As Toriyama *et al.* pointed out, the conducting plane shifts from the hexagonal layer to the layer perpendicular to the blue arrow in Fig. 4(b) [25]. Note that the anisotropy in the conductivity for HEX structure is very small compared to a typical layered material, $PdCoO_2$ [26]. Rather high anisotropy in the conductivity for low T 5X structure suggests the 3D to 2D transition in its electronic structure as well as the shift in conducting plane. Note that in the 2D plane of 5X structure, there is still large anisotropy in the conductivity, which is related to the direction of Ir dimer formation. The largest conductivity is along the axis (red arrow) shown in Fig. 4(a), along which no distinct dimerization occurs. Smallest conductivity is along the blue arrow, which is perpendicular to the dimer order planes of Ir and Te. The direction of the blue arrow is close to $q_{1/5} = (1/5,0,1/5)$, as shown in Fig. 4(b).

Oh *et al.* reported the resistivity data of $IrTe_2$ as a function of T [12]. The ratio of hexagonal in-plane conductivity and out-of-plane conductivity is about 6.4 for high T phase (HEX) of $IrTe_2$. It is far from the DFT result of $\sim$2.0. This difference might result from the constant relaxation time approximation used in BoltzTraP, and/or the experimental complexity to measure the resistivity along the c axis in the layered material. Moreover, at low T, it is hard to compare the experimental data and the theoretical results directly, because of the existence of domains in the low T phase of 5X. The orientation of domains and the effect of domain wall scattering will make the situation complicated.

IV. CONCLUSION

Using the DFT band calculations, we have simulated the optical spectra of $IrTe_2$ for several structures in the literature. The optical data calculated with 5X structure refined by Pascut *et al.* shows good agreement with experiment, which provides the structural identification of 5X at low T. Heavy reduction of reflectivity in the low frequency part indicates the substantial band reconstruction in the large window up to 1–2 eV around E_F. Comparing calculated optical spectra with experimental data reveals that Ir-Ir dimer formation is responsible for the low frequency optical spectra, which is corroborated by the analysis of the FS topology. We can also infer from the optical spectra that the reduction of metallicity occurs with the formation of dimer order. We also calculated electric conductivity within the Boltzmann transport theory. Obtained electrical conductivity tensor indicates the reduction of dimensionality, which is also closely related to partial gap opening along a specific direction, characterized by the disappearance of lobe of the Fermi surface.

ACKNOWLEDGMENTS

Fruitful discussions with K.-T. Ko are greatly appreciated. This work was supported by the NRF (Grant No. 2011-0025237), the POSTECH BSRI Grant, the National Creative Initiative (No. 2009-0081576), and KISTI (Grant No. KSC-2013-C3-064).

[1] J. A. Wilson and A. D. Yoffe, Adv. Phys. **18**, 193 (1969).
[2] J. A. Wilson, F. J. Di Salvo, and S. Mahajan, Adv. Phys. **24**, 117 (1975).
[3] K. Rossnagel, J. Phys. Condens. Matter **23**, 213001 (2011).
[4] M. Calandra and F. Mauri, Phys. Rev. Lett. **106**, 196406 (2011).

[5] K. E. Wagner, E. Morosan, Y. S. Hor, J. Tao, Y. Zhu, T. Sanders, T. M. McQueen, H. W. Zandbergen, A. J. Williams, D. V. West, and R. J. Cava, Phys. Rev. B. **78**, 104520 (2008).
[6] J. J. Yang, Y. J. Choi, Y. S. Oh, A. Hogan, Y. Horibe, K. Kim, B. I. Min, and S.-W. Cheong, Phys. Rev. Lett. **108**, 116402 (2012).
[7] D. Ootsuki, Y. Wakisaka, S. Pyon, K. Kudo, M. Nohara, M. Arita, H. Anzai, H. Namatame, M. Taniguchi, N. L. Saini, and T. Mizokawa, Phys. Rev. B **86**, 014519 (2012); D. Ootsuki, S. Pyon, K. Kudo, M. Nohara, M. Horio, T. Yoshida, A. Fujimori, M. Arita, H. Anzai, H. Namatame, M. Taniguchi, N L. Saini, and T. Mizokawa, Journal of Physics: Conference Series **428**, 012018 (2013).
[8] D. Ootsuki, S. Pyon, K. Kudo, M. Nohara, M. Horio, T. Yoshida, A. Fujimori, M. Arita, H. Anzai, H. Namatame, M. Taniguchi, N. L. Saini, and T. Mizokawa, J. Phys. Soc. Jpn. **82**, 093704 (2013).
[9] A. F. Fang, G. Xu, T. Dong, P. Zheng, and N. L. Wang, Sci. Rep. **3**, 1153 (2013).
[10] H. Cao, B. C. Chakoumakos, X. Chen, J. Yan, M. A. McGuire, H. Yang, R. Custelcean, H. Zhou, D. J. Singh, and D. Mandrus, Phys. Rev. B **88**, 115122 (2013).
[11] T. Qian, H. Miao, Z. J. Wang, X. Liu, X. Shi, Y. B. Huang, P. Zhang, N. Xu, P. Richard, M. Shi, M. H. Upton, J. P. Hill, G. Xu, X. Dai, Z. Fang, H. C. Lei, C. Petrovic, A. F. Fang, N. L. Wang, and H. Ding, arXiv:1311.4946v1.
[12] Y. S. Oh, J. J. Yang, Y. Horibe, and S.-W. Cheong, Phys. Rev. Lett. **110**, 127209 (2013).
[13] N. Matsumoto, K. Taniguchi, R. Endoh, H. Takano, and S. Nagata, J. Low Temp. Phys. **117**, 5, (1999); **117**, 1129 (1999).
[14] G. L. Pascut, K. Haule, M. J. Gutmann, S. A. Barnett, A. Bombardi, S. Artyukhin, T. Birol, D. Vanderbilt, J. J. Yang, S.-W. Cheong, and V. Kiryukhin, Phys. Rev. Lett. **112**, 086402 (2014).
[15] S. Jobic, R. Brec, and J. Rouxel, J. Solid State Chem. **96**, 169 (1992).
[16] K. Mizuno, K. Magishi, Y. Shinonome, T. Saito, K. Koyama, N. Matsumoto, and S. Nagata, Physica B **312-313**, 818 (2002).
[17] B. Joseph, M. Bendele, L. Simonelli, L. Maugeri, S. Pyon, K. Kudo, M. Nohara, T. Mizokawa, and N. L. Saini, Phys. Rev. B **88**, 224109 (2013).
[18] K. Kim, S. Kim, K.-T. Ko, H. Lee, J. H. Park, J. J. Yang, S.- W. Cheong, and B. I. Min (unpublished).
[19] M. J. Eom, K. Kim, Y. J. Jo, J. J. Yang, E. S. Choi, B. I. Min, J. H. Park, S.-W. Cheong, and J. S. Kim (unpublished).
[20] B. Li, G. Huang, J. Sun, and Z. Xing, Sci. Rep. **4**, 6433 (2014).
[21] P. Blaha, K. Schwarz, G. K. H. Madsen, D. Kvasnicka, and J. Luitz, WIEN2K, An Augmented Plane Wave + Local Orbitals Program for Calculating Crystal Properties (Karlheinz Schwarz, Techn. Universität Wien, Austria, 2001).
[22] C. Ambrosch-Draxl and J. Sofo, Comput. Phys. Commun. **175**, 1 (2006).
[23] G. K. H. Madsen and D. J. Singh, Comput. Phys. Commun. **175**, 67 (2006).
[24] G. Dresselhaus and M. S. Dresselhaus, *In The Optical properties of Solids*, edited by J. Tauc (Academic, New York, 1966), p. 13; D. Puggioni and J. M. Rondinelli, J. Phys. Condens. Matter **26**, 265501 (2014).
[25] T. Toriyama, M. Kobori, T. Konishi, Y. Ohta, K. Sugimotto, J. Kim, A. Fujiwara, S. Pyon, K. Kudo, and M. Nohara, J. Phys. Soc. Jpn. **83**, 033701 (2014).
[26] K. P. Ong, D. J. Singh, and P. Wu, Phys. Rev. Lett. **104**, 176601 (2010).